Variability in Output Characteristics of Single-Walled Carbon Nanotube Thin-Film Transistors

Jialuo Chen and Satish Kumar

***Abstract*—Single-walled carbon nanotube (CNT) based thin-film transistors (TFTs) are promising candidates for future electronic devices because of their excellent properties. However, device-to-device performance variability of TFTs can pose challenging problems, which is rooted in the randomness of CNT networks, the variation in individual CNT properties due to change in chirality, and the fabrication imperfections. This paper presents a systematic study of variability in *I–V* characteristics through a combination of experimental and theoretical analysis of the major sources that cause performance variation. The sources of variation including the percentage of metallic CNTs (m-CNTs), threshold voltage, CNT mean length, and CNT network density have been studied separately. The analysis shows that the presence of m-CNTs is a major source contributing to the performance variation for short channel TFTs, but its effect reduces for large channel length transistors. The threshold voltage is found to be the major source of variation for long channel TFTs. A better consistency in performance can be guaranteed for TFTs with larger channel area, which ensures a smaller variation in CNT network density and CNT mean length. These results provide key insights into the variability estimation of *I–V* characteristics of CNT-based devices, which is vital for reliability studies of CNT-TFTs based circuits for different electronic applications.**

***Index Terms*—Variability, carbon nanotube, thin film transistor, I–V characteristics.**

I. Introduction

SINGLE-WALLED carbon nanotube (SWCNT) thin film transistors (TFTs) have been widely investigated in the last decade. As a new generation of metal-oxide-semiconductor field-effect transistors (MOSFETs), they have significant advantages such as high operation speed [1], [2], low power consumption [2], and high flexibility [3], [4]. CNT-TFTs are also promising for flexible microelectronics applications because of their high mobility, substrate-neutrality, and low-temperature fabrication process [5]. As a one-dimensional material, SWCNTs have exceptional high current carrying capacity as its mobility can reach 100,000 $cm^2V^{-1}s^{-1}$ [6], [7]. Extraordinary flexibility [8]–[11] and elasticity [12] can also be expected when it undergoes high strain and bending. Aligned SWCNT based TFTs have certain advantages such as small TFT dimensions, high mobility, and only few CNTs are needed per channel. However, the removal of m-CNTs and cost-effective fabrication of these TFTs are still challenging. The CNT network based TFT is of high interest for low-cost and large area electronics such as antennae, RF tags, sensors, etc. as it is comparatively much easier to fabricate on both flexible and hard substrates [13]–[16]. In recent years, the cost of CNTs has significantly dropped and the large amount of CNT usage per TFT is not a major concern from a cost standpoint [6], [7].

Device-to-device performance variation of CNT-TFTs is becoming a critical problem while trying to harvest the exceptional properties of CNTs. Performance variations of TFTs can be reflected in the variability in I–V characteristics, including output and transfer characteristics. It results from the multiple sources. The atomic structure of a CNT is a source of large variation, which includes variations in length, diameter, defects, doping, etc. [17]. A CNT of similar diameter can be either metallic or semiconducting depending on its chirality, leading to significant variability in I–V characteristics. The CNT network distribution and morphology in its channel area, e.g., CNT network density, channel length, and orientation, are very different from one TFT to other because of the randomness induced during deposition [17]. Fabrication process, especially fabrication imperfections [18] further affect the variability.

In the previous studies [19]–[26], performance variation of CNT based field-effect transistors (FETs) had been discussed with respect to the CNT diameter [19], [20], CNT density fluctuation [21], CNT growth and manufacturing process [22]. Cao *et al*. studied variability in threshold voltage (V_{th}) of CNT-FETs. They showed that variability in V_{th} mainly results from the random fluctuation of fixed charges on the oxide/air interface [23], [24]. Franklin *et al*. analyzed the origin of variability in V_{th} and hysteresis of CNT-FETs, and tried to improve the device-to-device consistency through optimized gate dielectric and passivation layer [21]. Performance variability of FETs with aligned CNTs [19], [25], [26] was also of high interest, which had been studied in similar ways to achieve better consistency. However, most of the studies only focused on the devices using single or aligned nanotubes as channel. None of them reported the variability analysis of CNT-TFTs using random CNT networks as channel. For CNT networks, the variability analysis becomes more complicated due to randomness in the network structure and CNT distribution. Undoubtedly, these further increase performance uncertainty, which need to be analyzed and understood thoroughly.

Manuscript received November 8, 2017; revised January 5, 2018; accepted January 28, 2018. Date of publication February 7, 2018; date of current version March 8, 2018. The review of this paper was arranged by Associate Editor A. Ural. This work was supported by the NSF Grant CCF-1319935. *(Corresponding author: Jialuo Chen.)*

The authors are with The G. W. Woodruff School of Mechanical Engineering, Georgia Institute of Technology, Atlanta, GA 30332 USA (e-mail: jlchen@gatech.edu; satish.kumar@me.gatech.edu).

Digital Object Identifier 10.1109/TNANO.2018.2803106

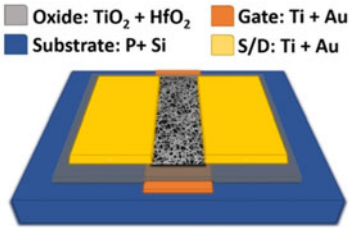

Fig. 1. Schematic of a CNT-TFT on a Si wafer.

In this work, both experimental and theoretical methods were employed to analyze the variability in I–V characteristics in a statistical framework. For the experimental analysis, we fabricated array of CNT-TFTs using high-k dielectric HfO_2 as gate oxide layer to achieve high performance. For the theoretical part, we applied the current scaling relationship developed by Pimparkar *et al*. [27] and analyzed each variable used in the relationship. Variation sources such as % of m-CNTs, V_{th}, CNT mean length, and CNT network density were studied statistically for different channel dimensions. For the first time, the variability analysis of random CNT network based TFTs has been studied systematically. This analysis presents an effective way of the variability estimation of CNT network based TFTs. Such analysis is crucial to explore the reliability and stability of CNT network based circuits and to devise techniques which can help reduce variability in circuit performance for various electronic applications.

II. Fabrication of CNT-TFTs

CNT-TFTs were fabricated at the Institute for Electronics and Nanotechnology (IEN) cleanroom at Georgia Tech. The structure of a typical TFT is illustrated in Fig. 1. TFTs were fabricated using photolithography and lift-off process [28]–[32]. First, Ti/Au (5 nm/50 nm) layers as back gate were deposited on top of a Si wafer by e-beam evaporation at deposit rate of 0.2 Å/s and 1 Å/s respectively. The gate contacts were patterned between the source/drain (S/D, deposited later) electrodes. Following this, atomic layer deposition (ALD) was used to deposit TiO_2 (1.5 nm/15 cycles) and HfO_2 (75 nm/600 cycles), covering the entire wafer surface as a global gate-dielectric layer. Ti and TiO_2 work as adhesion layers for the gate and gate dielectric. Then, 15 $\sim$ 30 s oxygen plasma treatment was indispensable to make the surface hydrophilic [33]. After this, CNT network was deposited by immersing the wafer into 0.005 $\sim$ 0.01 g/L toluene-based CNT solution for 5 $\sim$ 15 minutes (CNT source: >99% purity polymer-wrapped CNT solution from NanoIntegris). The resulting density of the CNT network is a function of both deposition time and concentration of the CNT solution. Scanning electron microscope (SEM) images of the CNT networks are shown in Fig. 2. Ti/Au (5 nm/50 nm) layers as S/D electrodes are patterned by photolithography and lift-off process. This step was followed by another photolithography and 30 s oxygen plasma treatment to form channel area by etching away unwanted part of the CNT network. At last, vacuum annealing at 250°C for 2 hours was performed to get rid of the surface residue on the wafer. The final surface features and a CNT network in the channel is exhibited in Fig. 3.

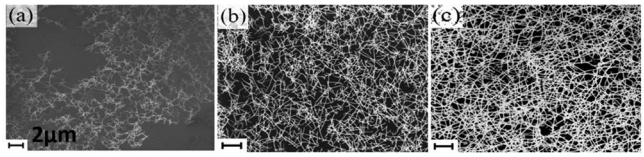

Fig. 2. SEM images of CNT networks fabricated using different recipes. CNT source: 99% high purity toluene-based CNT solution. All scale bars are 2 μm. (a) Concentration = 0.005 g/L, deposition time = 10 min, without any surface treatment. (b) Concentration = 0.005 g/L, deposition time = 10 min, with surface treatment (oxygen plasma treatment for 30 s). (c) Concentration = 0.01 g/L, deposition time = 10 min, with surface treatment.

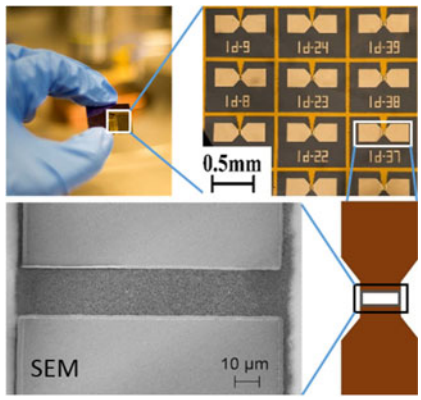

Fig. 3. Fabricated CNT-TFTs and the SEM image of CNT network in the channel area of a CNT-TFT.

The I–V characteristics of the CNT-TFTs had been measured using Microtech Summit 11 k probe station and Keithley 4200-SCS. We fabricated series of devices with the same channel width, but different channel lengths. The output characteristics ($I_d - V_{ds}$ curves) of the CNT-TFTs is depicted in Fig. 4(a) for different channel lengths with V_{ds} swept from 0 to -4 V at $V_{gs} = -1$ V. For the transfer characteristics ($I_d - V_{gs}$ curves), V_{gs} was swept from $-4 \sim 4$ V (forward sweeping) while keeping $V_{ds} = -1$ V. Semi-log plots are shown in Fig. 4(b) for each channel length. The on/off ratio increases from 10^3 to as high as 10^5 when the channel length increases from 5 μm to 60 μm, which can be expected since the CNT networks still contain m-CNTs even though it is purified for 99% semiconducting tubes. The on/off ratio is a function of the channel length as the TFTs with smaller channel length have much higher possibility to bridge the channel by m-CNTs. In Fig. 4(c), the output characteristics at different V_{gs} is plotted for a specific device. The overall I–V characteristics shows good performance of the p-type CNT-TFTs with on/off ratio as high as 10^5 and mobility around $1 \sim 4$ cm^{2}V^{-1}s^{-1}.

III. Results and Discussion

This study focuses on the variability analysis of I–V characteristics of CNT-TFTs. The performance variation resulting from the multiple sources is described below:

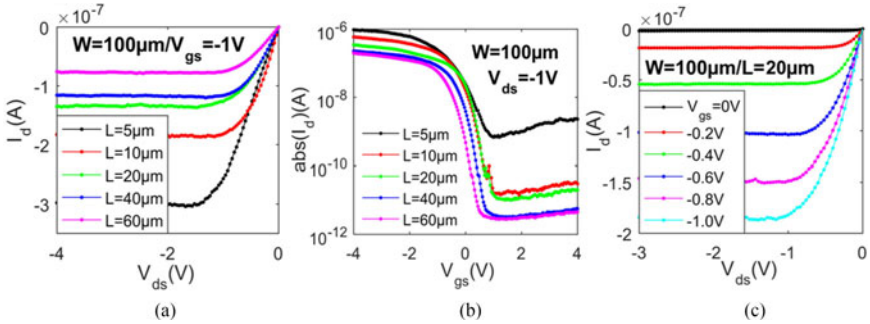

Fig. 4. I–V characteristics of CNT-TFTs fabricated at the IEN cleanroom. (a) Output characteristics (I_d–V_{ds} curves) of TFTs for various channel lengths (5 μm, 10 μm, 20 μm, 40 μm and 60 μm) measured at $V_{gs} = -1$ V; channel width (W = 100 μm) is same for all devices. (b) Transfer characteristics (I_d–V_{gs} curves) of the same TFTs as in (a) measured at $V_{ds} = -1$ V. (c) Output characteristics of a TFT (L = 20 μm, W = 100 μm) measured at different V_{gs} (0, −0.2, −0.4, −0.6, −0.8 and −1 V). All measurements were conducted by Cascade Microtech probe station and Keithley 4200-SCS.

1) On the Level of Individual CNTs

One of the major sources of variability lies in the large difference of electronic properties between m-CNTs and semiconducting CNTs (s-CNTs). Generally, as-grown CNT networks contains 33% m-CNTs, which largely limit the function of gate to achieve high on/off ratio [34]. In Fig. 4, the on/off ratio varies from 10^3 to 10^5 for different channel lengths even though 99% purified CNT solution (i.e., 99% s-CNT and 1% m-CNT) were used. The length distribution of CNT is another source of variability. In our CNT networks, the average length of CNT is $\sim$1 μm. However, some CNTs can be as long as 5 μm while some other CNTs can be as short as 0.1 μm. The performance variations for the short channel TFTs will be much higher since longer CNTs can directly bridge the source and drain with much higher probabilities [27]. Besides, difference in diameter, morphology, doping of individual CNTs may also contribute to the variability in I–V characteristics [35], [36].

2) On the Level of the CNT Networks

On the one hand, CNT network density has a significant effect on the drain current, which has been studied intensively in the recent years. The significant performance variations can result from the density variation since it cannot be controlled perfectly in practice. No matter how a CNT network is fabricated in a TFT, density will vary from region to region. On the other hand, CNT network structure can be another potential reason for variability. For TFTs with the same channel length and the same network density, performance variations will still exist because the randomly distributed CNTs make each network structure different from each other. Although each TFT has different network structure and details, certain statistical distribution may still follow. By studying TFTs with a range of channel dimensions and network densities, we can decipher the variability in a statistical framework.

3) On the Level of the Device

The variation in V_{th} can lead to significant variation in I–V characteristics and device performance. V_{th} can be obtained for each TFT and its effect on the variability can be quantified [37]–[39]. Many imperfections may exist during the fabrication process which can be significant sources of variation, e.g., variations in oxide layer thickness, contact patterns, contamination region by region etc.

In general, the sources described above at different levels can contribute to the final performance variation. It is impossible and needless to analyze each cause one by one. But capturing the effect of most important sources is rather reasonable and feasible. In this work, contact resistance (Rc) between CNTs and electrodes has been ignored because Rc is small compared to the total resistance (R_{SD}) of the random CNT networks considered. Using a transfer length method (TLM), Rc is estimated to be $\sim$6.8 kΩ which is less than 1% of the average RSD of the smallest channel length considered ($\sim$5 μm). The reason for high R_{SD} is rooted in the large number of CNT-CNT junctions inside a randomly generated CNT network, which dominates RSD. In the following discussion, variation in I–V characteristics of TFTs were analyzed and compared by both experimental and theoretical means. Experimental data corresponds to the I–V characteristics measured for the TFTs fabricated at Georgia Tech's IEN. Theoretical data were obtained using the empirical formula developed by Pimparkar *et al.* [27].

A. Output Characteristics

CNT-TFTs with three different channel length series (L = 5 μm, 10 μm, and 50 μm) were considered and referred as 5 μm series, 10 μm series, and 50 μm series, respectively. For each series, we fabricated 45 CNT-TFTs and analyzed the variability of I–V. The transfer and output characteristics was measured for CNT-TFTs with 5 μm, 10 μm, and 50 μm series (all with channel width of W = 100 μm). For output characteristics, V_{ds} was swept from 0 to −2 V at $V_{gs} = -1$ V. From Fig. 5(a)–(d), it is obvious that TFTs with longer channel lengths have smaller current magnitude, which is expected. It can be also noted that the longer channel TFTs have a smaller range of variation in the saturated current, referred as $I_{d(sat)}$. From the experimental data, the range of variation in $I_{d(sat)}$ of L = 5 μm, 10 μm, and 50 μm series are $(-1 \times 10^{-6}, -0.6 \times 10^{-7})$, $(-4 \times 10^{-7}, -0.5 \times 10^{-7})$, and $(-2.1 \times 10^{-7}, -0.4 \times 10^{-7})$. Their mean values are -2.8×10^{-7}, -1.7×10^{-7}, and -1.3×10^{-7} respectively. Here the unit of current is Ampere (A) by default unless

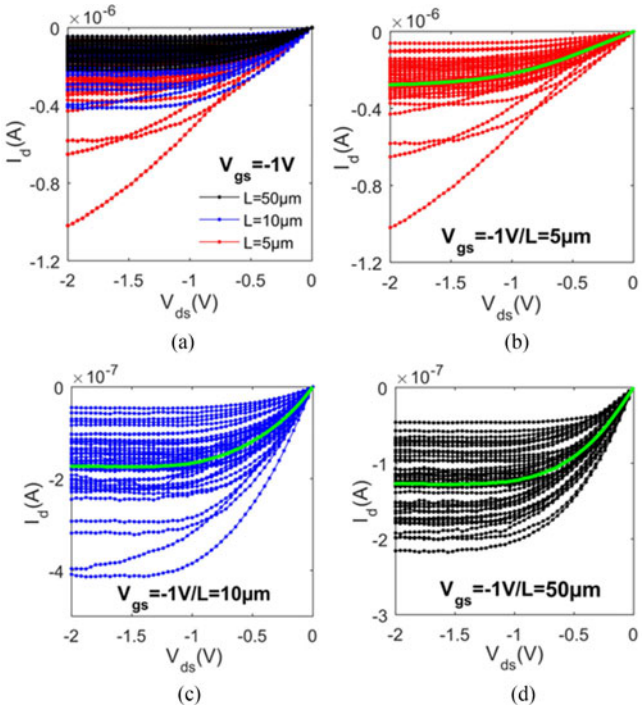

Fig. 5. Measured output characteristics of fabricated CNT-TFTs with various channel lengths (L series) but same channel width (W = 100 μm) at $V_{gs} = -1$ V. (a) Output characteristics of devices are shown together, and (b) separately for L series TFTs: 5 μm series, (c) 10 μm series, and (d) 50 μm series. Green curves in (b)–(d) denote average output characteristics.

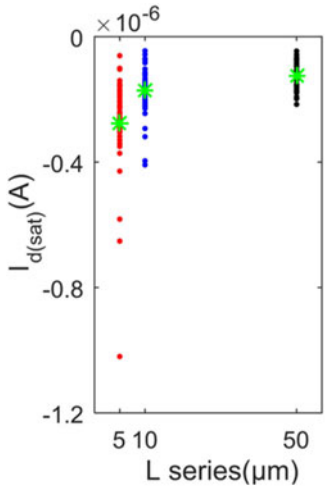

Fig. 6. $I_{d(sat)}$ distribution for various channel lengths. L series: red = 5 μm series; blue = 10 μm series, black = 50 μm series. Green stars denote average values for each series.

stated otherwise. For the TFTs whose current does not saturate in the range of sweep voltage considered, the $I_{d(sat)}$ corresponds to the maximum magnitude of the measured current. The average $I_d - V_{ds}$ curves for each series are illustrated in Fig. 5(b)–(d) by green curves. The $I_{d(sat)}$ distribution can be found in Fig. 6. The standard deviations for 5 μm, 10 μm, and 50 μm series are 1.7×10^{-7}, 7.7×10^{-8}, and 4.1×10^{-8}, respectively. And the corresponding standard deviation normalized by mean are 0.61, 0.45, and 0.32 respectively. From the experimental data, it can be deciphered that the longer channel length TFTs are more stable and have less variations in performance.

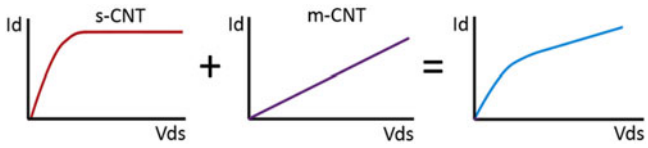

Fig. 7. Schematic of output characteristics for s-CNT, m-CNT, and considering mutual influence from both.

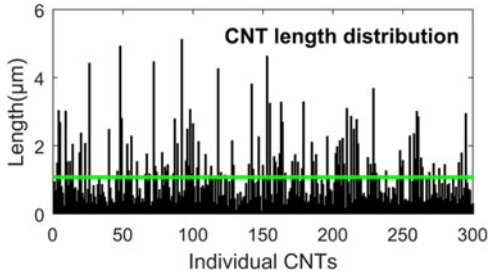

Fig. 8. CNT length distribution from measurement. A sample of 300 CNTs was chosen for statistics (x-axis). Green line denotes the average length (1.08 μm) of the 300 CNTs (reference average length $\sim$1 μm).

B. s-CNT and m-CNT

In experiments, the variability of I–V characteristics is a combined result of all possible sources. It is difficult to separate the influence of each source. However, the influence of some variables can be easily deciphered, e.g., m-CNTs and s-CNTs. As depicted in Fig. 7, the I–V curves are significantly different for TFTs with only m-CNTs or only s-CNTs. The presence of m-CNTs makes the curves unsaturated since m-CNTs form a percolating path through source and drain (the m-CNT effect). It will be difficult to switch on or switch off the transistor by gating. Considering this fact, we further inspected the curves in Fig. 5. Clearly, the m-CNT effect is significant only for 5 μm and 10 μm series, and insignificant for 50 μm series. As we used 99% purified CNT solution, it is very less likely that m-CNTs bridge source and drain with distance of 50 μm when the average length of CNTs is only 1 μm and the CNT network density is around $13/\mu m^2$. However, the probability is much higher for m-CNTs to bridge source and drain for 5 μm series TFTs. Moreover, there are some longer CNTs (3–5 μm, some even >5 μm) which will make bridging much easier for 5 μm series. In Fig. 8, CNT length distribution was investigated. The average length is 1.08 μm, which is consistent with the reference value $\sim$1 μm. That is why we have relatively large % of TFTs experiencing the m-CNT effect for 5 μm series, less for 10 μm series, none for 50 μm series. After ruling out the m-CNT effect (discard unsaturated curves), the variation range for 5 μm series is narrowed down from $(-10 \times 10^{-7}, -0.6 \times 10^{-7})$ to $(-4.3 \times 10^{-7}, -0.6 \times 10^{-7})$. While 10 μm and 50 μm series stay the same. Therefore, the m-CNT effect dominates performance variations for short channel TFTs but not for the long channel TFTs. Even though the m-CNT effect exists for 10 μm series, its variation range does not change.

To analyze other potential variation sources, we resort to the current scaling relationship [27], which does not include the

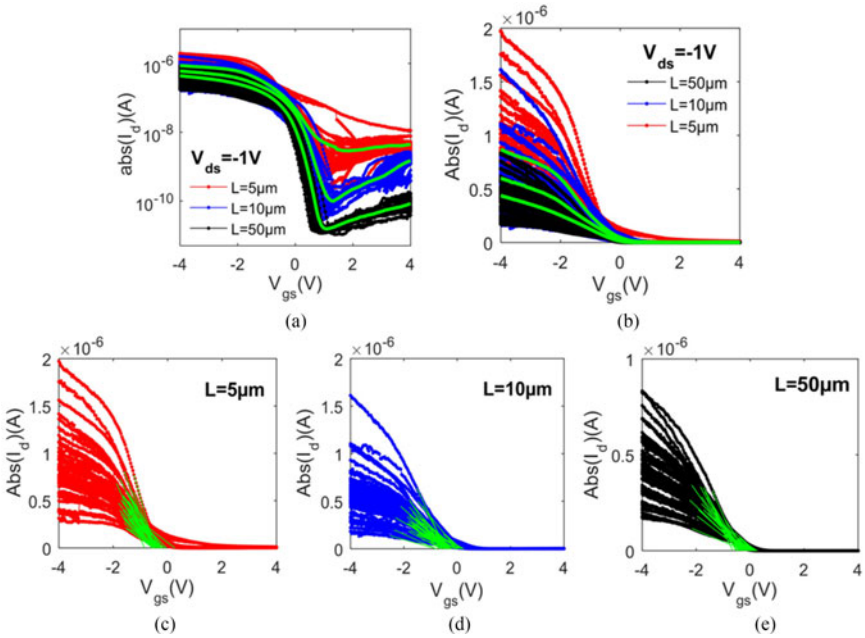

Fig. 9. Measured transfer characteristics using (a) semi-log scale and(b) linear scale of CNT-TFTs with various channel lengths (L series) but same channel width (W = 100 μm). V_{th} is estimated by extrapolation in linear region for (c) 5 μm series, (d) 10 μm series, and (e) 50 μm series. Green curves in (a)-(b) denote the average transfer characteristics for 5 μm, 10 μm, and 50 μm series respectively. Green lines in (c)–(e) denote the first derivative of each transfer characteristics used for V_{th} extrapolation.

effect of m-CNTs.

$$I_d = \frac{A}{L_S}\xi\left(\frac{L_S}{L}, \rho L_S^2\right) \times f\left(V_{\rm gs}, V_{\rm ds}\right) \tag{1}$$

Here, I_d is the drain current and the proportionally constant A depends on the oxide capacitance, CNT diameter and CNT-CNT interaction parameter [39]. Ls is CNT mean length. ξ and f are functions of the geometrical parameters (Ls, L and ρ) and bias conditions (V_{gs} and V_{ds}), where L is channel length, ρ is CNT network density, V_{gs} is gate bias voltage, and V_{ds} is drain bias voltage. ξ can be expressed as

$$\xi\left(\frac{L_S}{L}, \rho L_S^2\right) = \left(\frac{L_S}{L}\right)^{m(\rho L_S^2)} \tag{2}$$

Here m is a universal exponent of CNT percolating system, which is a function of ρ and Ls. This relation is derived and analyzed in [27]. The bias-dependent scaling function

$$f(V_{\rm gs}, V_{\rm ds}) = \left[(V_{\rm gs} - V_{\rm th})V_{\rm ds} - \frac{1}{2}V_{\rm ds}^2\right] \tag{3}$$

is independent of the geometrical parameters, where V_{th} is threshold voltage. Plugging (2) and (3) into (1), the current scaling relationship can be expressed as

$$I_d = \frac{A}{L_S}\left(\frac{L_S}{L}\right)^m \left[(V_{\rm gs} - V_{\rm th})V_{\rm ds} - \frac{1}{2}V_{\rm ds}^2\right] \tag{4}$$

Theoretically, all the listing variables will have effects on the variation of I_d. By considering each variable as a statistical distribution such as normal or lognormal distribution, the corresponding distribution for I_d can be obtained.

C. Threshold Voltage

The V_{th} distribution was considered as a source of variability in the I–V characteristics. Ortiz-Conde *et al*. studied multiple methods to obtain V_{th} from the transfer characteristics [38], e.g., by linear extrapolation of the $I_d - V_{gs}$ curve at its maximum first derivative point and finding the intercept of the gate bias axis. Using this method, we extracted V_{th} from the measured $I_d - V_{gs}$ curves where V_{gs} was swept from $-4\sim4$ V at $V_{ds} = -1$ V. $I_d - V_{gs}$ curves are shown in Fig. 9(a) and (b) under both linear and semi-log axes for V_{gs}. The results for V_{th} are presented in Fig. 9(c)–(e) for 5 μm, 10 μm, and 50 μm series separately. The corresponding distribution of V_{th} can be found in Fig. 10. Average V_{th} equals to -0.39 V, -0.25 V, and -0.13 V, and standard deviation of V_{th} equals to 0.17, 0.25, and 0.23 for 5 μm, 10 μm, and 50 μm series, respectively. Even though V_{th} shows increasing trend with increasing channel length, such trend should not be generalized for other TFTs. We do not have experimental data and evidences to accurately explain the physics behind this observation. V_{th} can be affected by many factors such as random dopant fluctuation, different types of oxide charges, body effect, etc. and the observed trend can be a combined influence of these parameters. V_{th} can be represented as a normal distribution, which is shown in inset of Fig. 10. Using the V_{th} distribution estimated from the experimental data, we obtained series of output characteristics from (4) by setting the rest of variables constants (Ls = 1.08 μm, $V_{gs} = -1$ V, m = 1.05, L = 5 μm, 10 μm, and 50 μm for each series). Ls = 1.08 μm is CNT mean length, and m = 1.05 is determined by average CNT network density, which is $\mu = 13/\mu{\rm m}^2$. The value of A in (4) was determined by making the calculated average $I_{d(sat)}$ from (4) equals the experimental aver-

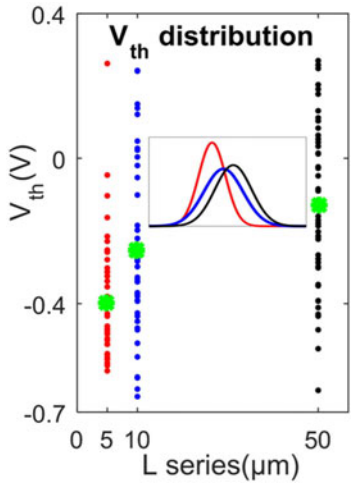

Fig. 10. V_{th} distributions for different L series extracted from Fig. 9. The curves in inset are the corresponding normal distributions: red = 5 μm, blue = 10 μm, black = 50 μm.

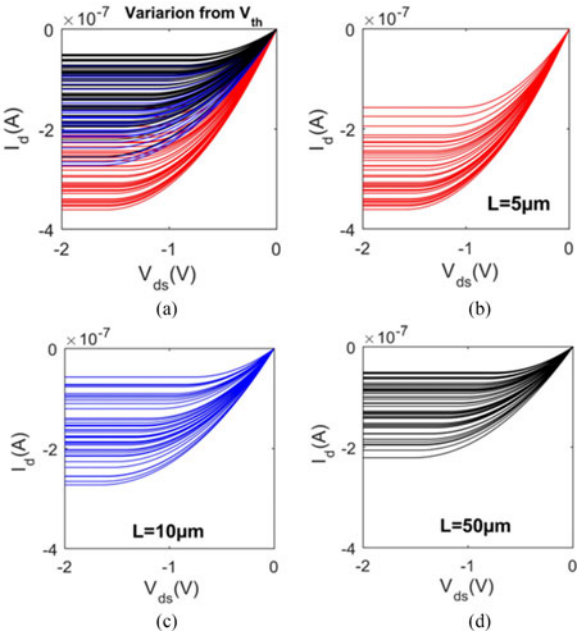

Fig. 11. The variability of output characteristics based on the normal distributions of V_{th}. (a) Three L series shown together for the same range. (b)–(d) 5 μm, 10 μm, and 50 μm series respectively.

age $I_{d(sat)}$. Therefore, V_{th} is the only source of variation in (4). The corresponding variability in output characteristics is shown in Fig. 11. The variation range of calculated $I_{d(sat)}$ for 5 μm, 10 μm and 50 μm series are $(-3.61 \times 10^{-7}, -1.57 \times 10^{-7})$, $(-2.73 \times 10^{-7}, -5.69 \times 10^{-8})$ and $(-2.21 \times 10^{-7}, -5.23 \times 10^{-8})$. Analyzing the measured $I_{d(sat)}$ in Fig. 6, the variation caused by V_{th} account for 16%, 61%, and 99% of the range of variation in $I_{d(sat)}$ for 5 μm, 10 μm, and 50 μm series, respectively. Therefore, V_{th} is a main source that contributes to variability in $I_{d(sat)}$ for long channel TFTs (L$>=$ 10 μm). While for short channel TFTs (L$<=$ 5 μm), V_{th} only accounts for a small part of the entire variation.

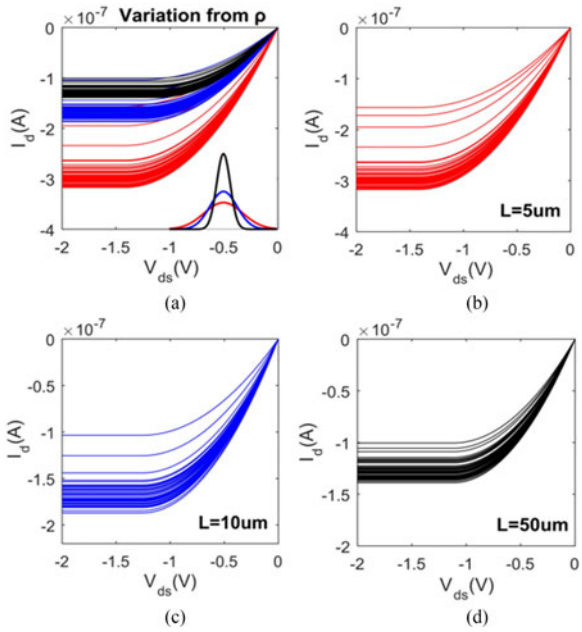

Fig. 12. The variability of output characteristics based on the normal distributions of CNT network density. (a) Three L series shown together for the same range. Inset represents the normal distribution of network density, red = 5 μm, blue = 10 μm, black = 50 μm. (b)–(d) Different L series for 5 μm, 10 μm, and 50 μm respectively.

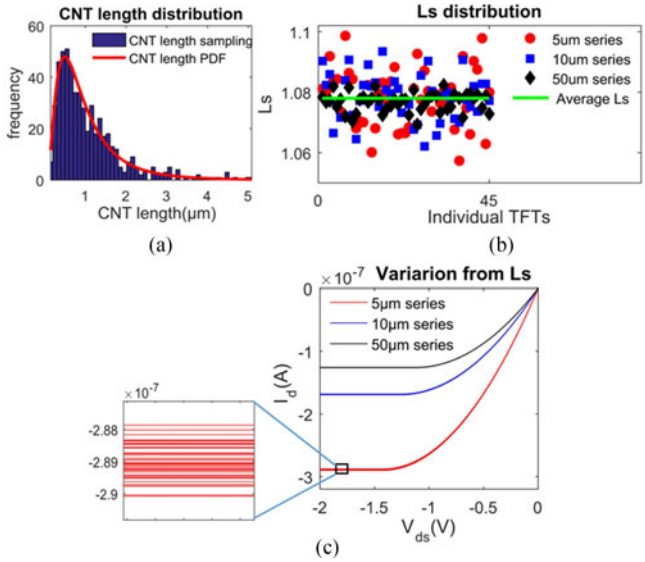

Fig. 13. (a) CNT length distribution measured by sampling from a low density CNT network and the fitted PDF of the CNT length. (b) Ls distribution for individual TFTs of each series. The green line denotes the average Ls of all series. (c) The variability in output characteristics is based on Ls.

D. CNT Network Density

The effect of CNT density (ρ) distribution in the TFT channel was analyzed using the same method as for V_{th}. The variation in ρ will result in the variation in 'm' parameter in Equation (4), which in turn affects the variability in output characteristics. The relationship between ρ and m can be found in [27]. From this relationship, we incorporated the distribution of ρ for each channel length series. Assume ρ obeys normal distribution with mean value μ and standard deviation σ, we measured ρ from

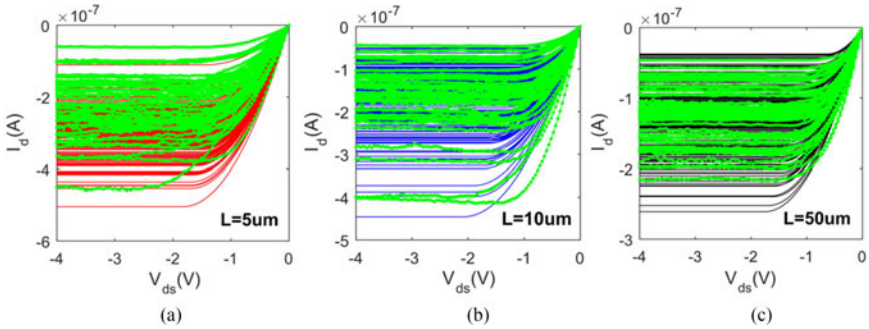

Fig. 14. The variability in output characteristics for (a) 5 μm series, (b) 10 μm series, and (c) 50 μm series based on normal distributions of threshold voltage (V_{th}), normal distribution of CNT network density (ρ), and lognormal distribution of CNT length (Ls). Green curves with dots are experimental data from the fabricated TFTs, same as Fig. 5 except the curves for TFTs with m-CNT effect are removed.

SEM images by sampling multiple regions inside TFT channels. This measurement was performed only for 5 μm series TFTs; we obtained statistical mean $\mu = 13/\mu m^2$ and standard deviation $\sigma = 2.45$. Based on this normal distribution, density values for all 5 μm TFTs were generated. This normal distribution for 5 μm series was then used for density value generation for 10 μm and 50 μm series. The only difference is, a 10 μm channel can be treated as two 5 μm-channels combined together and a 50 μm channel can be treated as ten 5 μm-channels combined together, with each element (a 5 μm-channel) obeys the same normal distribution with $\mu = 13$ and $\sigma = 2.45$. In this way, we can expect that the density for 10 μm and 50 μm series will stay the same ($13/\mu m^2$) as for 5 μm series while the standard deviation will be smaller. Both theoretical method and numerical sampling verified that the resulting standard deviations are $\sigma = 1.73$ for 10 μm series and $\sigma = 0.77$ for 50 μm series. Using the corresponding density distributions for 5 μm, 10 μm, and 50 μm series (Fig. 12 inset), the variability in output characteristics for each series was calculated and is presented in Fig. 12(a)–(d). Apparently, the range of variation for 5 μm, 10 μm, and 50 μm series decreases with the increasing channel length, which is in agreement with the experimental trends depicted in Fig. 5. This is because TFTs with larger channel area (longer channel lengths) are likely to have smaller standard deviation in density. Consequently, for 10 μm and 50 μm series, the range of variation caused by ρ are comparably smaller than that caused by V_{th}. But the range of variation for 5 μm series is at the same level. Therefore, the influence on the output characteristics variability from ρ is more prevalent for small channel length TFTs. But for long channel length TFTs, such influence is a secondary consideration.

E. CNT Mean Length

Using the similar method as for V_{th}, we considered the distribution of CNT mean length (Ls) in the channel area of TFTs. V_{th} can be extracted from I_d–V_{gs} curves while it is very difficult to obtain the length information of all CNTs in the TFT channel, especially when CNT network density is as large as $13/\mu m^2$. There will be a large number of CNTs in the channel and some CNTs may bundle with each other. So, a low density network was fabricated and the length of all CNTs in the network were recorded. We fitted the probability distribution function (PDF) to the measured CNT lengths, shown in Fig. 13(a). This was found to be a log-normal distribution as observed in some previous studies [40]. Based on this PDF, CNT networks were generated using a computational model for TFT series with different channel lengths at a given density. Then Ls was determined by averaging the CNT lengths for each TFT channel. This simulation method is statistically reasonable because the CNT networks in the fabricated TFTs were also randomly generated during deposition. Ls distributions for 5 μm, 10 μm and 50 μm series are plotted in Fig. 13(b), which clearly shows that the standard deviation is larger for shorter channels. As more CNTs exist in the longer channel TFTs at a given density, the mean CNT length (Ls) has a smaller range of variation than the channel with less CNTs. Based on the Ls distributions, the corresponding output characteristics were obtained and shown in Fig. 13(c). Results show that Ls has very limited influence on the variability due to the large number of CNTs in the channel. However, the influence from Ls will be much larger when density goes down in small channels, i.e., when the variation range of Ls will be much larger.

F. Comprehensive Effect of V_{th}, ρ, and Ls

Up to now, each important parameter of (4) has been considered individually. In practice, I–V characteristics variability is a comprehensive effect caused by all parameters. Therefore, we considered the comprehensive variations from V_{th}, network density (ρ), and CNT mean length (Ls) all together in Equation (4). To calculate the overall variability in I_d, V_{th}, ρ, and Ls were assigned values following their distribution functions (V_{th} and ρ satisfy normal distribution; Ls is based on the log-normal distribution of CNT length). We considered 200 samples in order to obtain a general variability of the output characteristics. Results are shown in Fig. 14(a)–(c). We observed that $I_{d(sat)}$ of more than 90% of samples fall into the variation range of $(-4.5 \times 10^{-7}, -1 \times 10^{-7})$, $(-4 \times 10^{-7}, -0.5 \times 10^{-7})$, and $(-2.5 \times 10^{-7}, -0.4 \times 10^{-7})$ for 5 μm, 10 μm, and 50 μm series respectively, compared with the experimental data in Fig. 5 (after removal of the curves with the m-CNT effect). Variation range comparison analyzed in Section III is illustrated in Fig. 15. It can be concluded that more than 90% of the variation range of simulation data overlap with the experimental data for each series. Therefore, the method applied here for variability analysis is reliable. It is an important tool to capture the overall variabil-

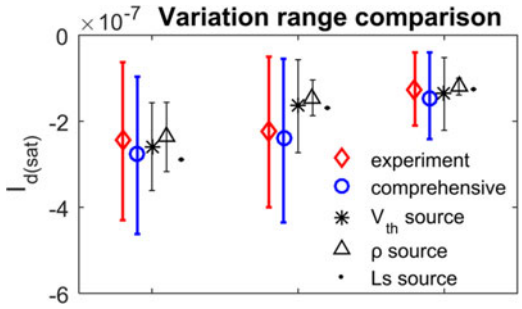

Fig. 15. Comparison of variation range of different sources (V_{th}, ρ, and Ls) individually, comprehensive effect of the three sources, and experimental measurement (without m-CNT effect) for three different series (L = 5 μm, 10 μm, and 50 μm) analyzed in Section III.

ity of CNT-TFTs, which can be further used in the design of relevant microelectronics.

IV. Conclusion

We fabricated array of CNT-TFTs of different channel lengths, and analyzed variability in the output characteristics through a combination of experimental and computational methods. We obtained distribution functions for different sources of variation such as threshold voltage, CNT network density and CNT mean length. The variability in I–V characteristics resulting from each source was analyzed individually and combined. The m-CNTs are found to be a major source contributing to variability in I–V characteristics for short channel TFTs. Threshold voltage is the major source of variation for long channel TFTs. The effect of variation in the CNT mean length can be ignored unless CNT network density is very low and channel is short. A better consistency in performance can be reached for TFTs with larger channel area, which ensure smaller variations in the CNT network density and the CNT mean length. More importantly, the variability of I–V characteristics for CNT-TFTs can be reconstructed from the distribution functions of the relevant parameters, which will be helpful for the reliability analysis and testing of CNT-TFT based devices and circuits.

References

[1] B. Kim, S. Jang, M. L. Geier, P. L. Prabhumirashi, M. C. Hersam, and A. Dodabalapur, "High-speed, inkjet-printed carbon nanotube/zinc tin oxide hybrid complementary ring oscillators," *Nano Lett.*, vol. 14, no. 6, pp. 3683–3687, 2014.

[2] A. Raychowdhury and K. Roy, "Carbon nanotube electronics: design of high-performance and low-power digital circuits," *IEEE Trans. Circuits Syst. I, Reg. Papers*, vol. 54, no. 11, pp. 2391–2401, Nov. 2007.

[3] C. M. Homenick *et al.*, "Fully printed and encapsulated SWCNT-Based thin film transistors via a combination of R2R gravure and inkjet printing," *ACS Appl. Mater. Interfaces*, vol. 8, no. 41, pp. 27900–27910, 2016.

[4] P. N. Nirmalraj, P. E. Lyons, S. De, J. N. Coleman, and J. J. Boland, "Electrical connectivity in single-walled carbon nanotube networks," *Nano Lett.*, vol. 9, no. 11, pp. 3890–3895, 2009.

[5] E. Artukovic, M. Kaempgen, D. Hecht, S. Roth, and G. Grüner, "Transparent and flexible carbon nanotube transistors," *Nano Lett.*, vol. 5, no. 4, pp. 757–760, 2005.

[6] T. Dürkop, S. Getty, E. Cobas, and M. Fuhrer, "Extraordinary mobility in semiconducting carbon nanotubes," *Nano Lett.*, vol. 4, no. 1, pp. 35–39, 2004.

[7] L. Hu, D. S. Hecht, and G. Gruner, "Carbon nanotube thin films: fabrication, properties, and applications," *Chem. Rev.*, vol. 110, no. 10, pp. 5790–5844, 2010.

[8] Y. Deng, M. Chan, and M. Zhang, "Fully transparent solution-processed carbon nanotube thin film transistors on a flexible substrate," in *Proc. 2016 IEEE 16th Int. Conf. Nanotechnol.*, 2016, pp. 299–302.

[9] K. Takei, "High performance, flexible CMOS circuits and sensors toward wearable healthcare applications," in *Proc. 2016 IEEE Int. Electron Devices Meeting*, 2016, pp. 6.1.1–6.1.4.

[10] Y. Zhao *et al.*, "Three-dimensional flexible complementary metal-oxide-semiconductor logic circuits based on two-layer stacks of single-walled carbon nanotube networks," *ACS Nano*, vol. 10, no. 2, pp. 2193–2202, 2016.

[11] B. Tian *et al.*, "Carbon nanotube thin film transistors fabricated by an etching based manufacturing compatible process," *Nanoscale*, vol. 76, pp. 4388–4396, 2017.

[12] B. I. Yakobson, C. Brabec, and J. Bernholc, "Nanomechanics of carbon tubes: instabilities beyond linear response," *Phys. Rev. Lett.*, vol. 76, no. 14, 1996, Art. no. 2511.

[13] P. Bondavalli, L. Gorintin, G. Feugnet, G. Lehoucq, and D. Pribat, "Selective gas detection using CNTFET arrays fabricated using air-brush technique, with different metal as electrodes," *Sensors Actuators B, Chem.*, vol. 202, pp. 1290–1297, 2014.

[14] K. Chen *et al.*, "Printed carbon nanotube electronics and sensor systems," *Adv. Mater.*, vol. 28, no. 22, pp. 4397–4414, 2016.

[15] K. Melzer *et al.*, "Enzyme assays using sensor arrays based on ion-selective carbon nanotube field-effect transistors," *Biosensors Bioelectron.*, vol. 84, pp. 7–14, 2016.

[16] F. Rigoni *et al.*, "Enhancing the sensitivity of chemiresistor gas sensors based on pristine carbon nanotubes to detect low-ppb ammonia concentrations in the environment," *Analyst*, vol. 138, no. 24, pp. 7392–7399, 2013.

[17] A. Jorio, E. Kauppinen, and A. Hassanien, "Carbon-nanotube metrology," *Carbon Nanotubes*, vol. 111, pp. 63–100, 2008.

[18] C. G. Almudever and A. Rubio, "Variability and reliability analysis of CNFET technology: Impact of manufacturing imperfections," *Microelectron. Rel.*, vol. 55, no. 2, pp. 358–366, 2015.

[19] A. E. Islam, F. Du, X. Ho, S. Hun Jin, S. Dunham, and J. A. Rogers, "Effect of variations in diameter and density on the statistics of aligned array carbon-nanotube field effect transistors," *J. Appl. Phys.*, vol. 111, no. 5, 2012, Art. no. 054511.

[20] H. Shahidipour, Y. Zhong, A. Ahmadi, and K. Maharatna, "Effects of CNT diameter variability on a CNFET-based SRAM," in *Proc. 2010 IEEE Asia Pac. Conf. Circuits Syst.*, 2010, pp. 971–974.

[21] C. G. Almudéver and A. Rubio, "Variability and reliability analysis of CNFET in the presence of carbon nanotube density fluctuations," in *Proc. 2012 19th Int. Conf. Mixed Des. Integr. Circuits Syst.,* 2012, pp. 124–129.

[22] C. G. Almudéver and A. Rubio, "Carbon nanotube growth process-related variability in CNFETs," in *Proc. 2011 11th IEEE Conf. Nanotechnol.*, 2011, pp. 1084–1087.

[23] Q. Cao *et al.*, "Origins and characteristics of the threshold voltage variability of quasiballistic single-walled carbon nanotube field-effect transistors," *ACS Nano*, vol. 9, no. 2, pp. 1936–1944, 2015.

[24] Q. Cao, J. Tersoff, S.-J. Han, and A. V. Penumatcha, "Scaling of device variability and subthreshold swing in ballistic carbon nanotube transistors," *Phys. Rev. Appl.*, vol. 4, no. 2, 2015, Art. no. 024022.

[25] A. D. Franklin *et al.*, "Variability in carbon nanotube transistors: Improving device-to-device consistency," *ACS Nano*, vol. 6, no. 2, pp. 1109–1115, 2012.

[26] N.-P. Wang, S. Heinze, and J. Tersoff, "Random-telegraph-signal noise and device variability in ballistic nanotube transistors," *Nano Lett.*, vol. 7, no. 4, pp. 910–913, 2007.

[27] N. Pimparkar, Q. Cao, S. Kumar, J. Murthy, J. Rogers, and M. Alam, "Current–Voltage characteristics of long-channel nanobundle thin-film transistors: A "bottom-up" perspective," *IEEE Electron Device Lett.*, vol. 28, no. 2, pp. 157–160, Feb. 2007.

[28] S. Cong *et al.*, "Carbon nanotube macroelectronics for active matrix polymer-dispersed liquid crystal displays," *ACS Nano*, vol. 10, no. 11, pp. 10068–10074, 2016.

[29] C. Wang *et al.*, "Extremely bendable, high-performance integrated circuits using semiconducting carbon nanotube networks for digital, analog, and radio-frequency applications," *Nano Lett.*, vol. 12, no. 3, pp. 1527–1533, 2012.

[30] J. Xia *et al.*, "Metal contact effect on the performance and scaling behavior of carbon nanotube thin film transistors," *Nanoscale*, vol. 8, no. 19, pp. 9988–9996, 2016.

[31] Y. Zou *et al.*, "Fabrication of all-carbon nanotube electronic devices on flexible substrates through CVD and transfer methods," *Adv. Mater.*, vol. 25, no. 42, pp. 6050–6056, 2013.

[32] G. Li *et al.*, "Fabrication of air-stable n-type carbon nanotube thin-film transistors on flexible substrates using bilayer dielectrics," *Nanoscale*, vol. 7, no. 42, pp. 17693–17701, 2015.
[33] Y. Wang, S. K. R. Pillai, and M. B. Chan-Park, "High-Performance partially aligned semiconductive single-walled carbon nanotube transistors achieved with a parallel technique," *Small*, vol. 9, no. 17, pp. 2960–2969, 2013.
[34] R. Martel, T. Schmidt, H. Shea, T. Hertel, and P. Avouris, "Single-and multi-wall carbon nanotube field-effect transistors," *Appl. Phys. Lett.*, vol. 73, no. 17, pp. 2447–2449, 1998.
[35] D. M. Sun, C. Liu, W. C. Ren, and H. M. Cheng, "All-carbon thin-film transistors as a step towards flexible and transparent electronics," *Adv. Electron. Mater.*, vol. 2, 2016, Art. no. 1600229.
[36] M. Y. Timmermans *et al.*, "Effect of carbon nanotube network morphology on thin film transistor performance," *Nano Res.*, vol. 5, no. 5, pp. 307–319, 2012.
[37] K. Navi, M. Rashtian, A. Khatir, P. Keshavarzian, and O. Hashemipour, "High speed capacitor-inverter based carbon nanotube full adder," *Nanoscale Res. Lett.*, vol. 5, no. 5, pp. 859–862, 2010.
[38] A. Ortiz-Conde, F. G. Sánchez, J. J. Liou, A. Cerdeira, M. Estrada, and Y. Yue, "A review of recent MOSFET threshold voltage extraction methods," *Microelectron. Rel.*, vol. 42, no. 4, pp. 583–596, 2002.
[39] X. Zhou, J.-Y. Park, S. Huang, J. Liu, and P. L. McEuen, "Band structure, phonon scattering, and the performance limit of single-walled carbon nanotube transistors," *Phys. Rev. Lett.*, vol. 95, no. 14, 2005, Art. no. 146805.
[40] S. Wang, Z. Liang, B. Wang, and C. Zhang, "Statistical characterization of single-wall carbon nanotube length distribution," *Nanotechnology*, vol. 17, no. 3, 2006, Art. no. 634.

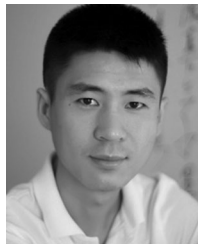

Jialuo Chen received the B.S. degree from the University of Shanghai for Science and Technology, Shanghai, China, in 2010, and the M.S. degree from Shanghai Jiao Tong University, Shanghai, China, in 2013, both in mechanical engineering. He is currently working toward the Ph.D. degree in electrical and computer engineering at the Georgia Institute of Technology, Atlanta, GA, USA. His current research focuses on fabrication and analysis of carbon nanotube network thin-film transistors.

Satish Kumar received the Ph.D. degree in mechanical engineering from Purdue University, West Lafayette, IN, USA, in 2007. He is currently an Associate Professor with the George W. Woodruff School of Mechanical Engineering, Georgia Institute of Technology, Atlanta, GA, USA. He has authored or coauthored more than 50 journal publications. He was a recipient of the 2012 Summer Faculty Fellowship from the Air Force Research Laboratories, the 2013 Woodruff School Teaching Fellowship, the 2014 DARPA Young Faculty Award, and the 2014 Sigma Xi Young Faculty Award.